Phase Formation in Calcium Oxide-Aluminosilicate Clay System

Nadjet Aklouche[1,2, a)]

[1] *Laboratory for the Development of New Materials and Their Characterization*
[2] *Faculty of Technology, Université Ferhat Abbas Sétif 1, Sétif 19000, Algeria*

[a)] Corresponding author: nadjet.aklouche@univ-setif.dz

Abstract. This study investigates the formation and structural evolution of calcium aluminosilicate (CAS) ceramics synthesized from Algerian halloysite and calcium hydroxide. Controlled heat treatments and analytical techniques, including X-ray diffraction (XRD), differential thermal and thermogravimetric analysis (DTA-TG), and Fourier transform infrared spectroscopy (FTIR), were employed to examine phase development and thermal stability. Highly crystalline anorthite was detected at temperatures as low as 1000 °C, achieved without external dopants or fluxing agents. When compared with recent literature, the proposed synthesis route exhibits notable advantages in terms of process simplicity, compositional purity, and raw material sustainability. This work highlights the potential of locally sourced clays as efficient precursors for functional CAS ceramics and provides a framework for benchmarking natural clay-based systems against advanced ceramic materials

INTRODUCTION

Calcium aluminosilicate (CAS) ceramics within the CaO-Al_2O_3-SiO_2 system have gained increasing attention for their outstanding thermal, chemical, and mechanical properties. These materials serve in applications requiring dimensional stability at elevated temperatures, such as metallurgical linings, refractory coatings, and aerospace components. Among the various crystalline phases, anorthite ($CaAl_2Si_2O_8$) stands out due to its high density, low thermal expansion and economic synthesis potential.

Despite significant research progress, the synthesis of pure CAS phases remains challenging. Many established methods depend on synthetic reagents, flux additives, or high-temperature treatments, limiting reproducibility and scalability. In resource-limited settings, these constraints hinder the adoption of advanced ceramic technologies. Consequently, attention has shifted toward exploiting abundant natural minerals particularly clays and feldspathic materials as alternative sources for oxide precursors.

Halloysite, a hydrated aluminosilicate with nanotubular morphology and reactive surface sites, represents a promising candidate for CAS formation. Its combination with calcium oxide precursors provides a simple, cost-effective, and environmentally responsible route for ceramic synthesis.

The present study explores the direct reaction between Algerian halloysite and calcium hydroxide to produce CAS ceramics through conventional heating, without chemical additives or dopants. Emphasis is placed on identifying phase formation pathways, structural transformations, and crystallization behavior using XRD, DTA-TG, and FTIR analyses. Comparative evaluation with recent publications demonstrates that, when appropriately processed, local clay resources can yield ceramics exhibiting crystallinity and performance comparable to those derived from synthetic systems.

This work therefore bridges experimental characterization with sustainable processing, contributing to a broader understanding of how natural raw materials can underpin next-generation aluminosilicate ceramics suitable for industrial deployment in Algeria and beyond.

MATERIALS AND METHODS

Raw Materials

The ceramic system examined in this study was developed from two primary natural sources. The first raw material was Algerian halloysite, collected from the *Jabal Debagh* deposit in Guelma, located in northeastern Algeria. This clay served as the main provider of alumina and silica for the $CaO–Al_2O_3–SiO_2$ (CAS) system. Prior to its use, the halloysite sample underwent structural and chemical characterization through X-ray diffraction (XRD), Fourier-transform infrared spectroscopy (FTIR), and thermal analysis (DTA–TG) to assess its purity, mineral phases, and thermal behavior (see *Fig. 1 a–c*).

The results confirmed that the sample was primarily composed of halloysite with minor accessory minerals. The principal chemical constituents identified in the raw material are summarized in Table 1, highlighting its suitability as a natural aluminosilicate precursor for ceramic synthesis.

TABLE 1. Chemical composition of Algerian halloysite used as raw material.

Oxide	**Symbol**	**Content(Wt.%)**
Silica	SiO_2	53.05
Alumina	Al_2O_3	44.41
Ferric oxide	Fe_2O_3	00.06
Calcium oxide	CaO	00.17
Manganese oxide	MnO	01.54

The chemical formula of Halloysite is $Al_2Si_2O_5(OH)_4$ characterized by its gray color due to the presence of MnO in its main components (1.54%), it also contains a large amount of SiO_2 (53.05%), followed by Al_2O_3 (44.41 %), these components are more important than its other components.

- Calcium oxide was used as the calcium source. Calcium oxide (CaO) was obtained from the Bounouara deposit in Constantine city in the east of Algeria, in the form of calcium carbonate stones $Ca(CO_3)$. The measured density was around 2.68 g/cm³, which equals to 98.90% of the theoretical density.

  After breaking the $Ca(CO_3)$ into small pieces, we calcined it in an electric furnace at 900 °C for 12 hours to release calcium oxide according to the following reaction:

$$Ca(CO_3) \longrightarrow CaO + CO_2$$

- **Ternary Diagramme $Cao\text{-}Al_2O_3\text{-}Sio_2$**

The ternary phase diagram is a graphical tool that illustrates the phase relationships in three-component systems at various compositions and temperatures. It is widely used in materials science to understand the interactions and stability of different phases.

Figure 1 shows the ternary phase diagram of the $CaO\text{-}Al_2O_3\text{-}SiO_2$ system. Based on the oxide content calculated from the composition of halloysite and CaO, the following values were obtained: 16.4 wt% CaO, 45.5 wt% Al_2O_3, and 38.1 wt% SiO_2.

These values were plotted on the diagram using the standard method of drawing lines parallel to the opposing axes:

- A line is drawn at 16.4 wt% along the CaO axis (parallel to the $Al_2O_3\text{-}SiO_2$ side),
- Another at 45.5 wt% along the Al_2O_3 axis (parallel to $CaO\text{-}SiO_2$),
- And a third at 38.1 wt% along the SiO_2 axis (parallel to $CaO\text{-}Al_2O_3$).

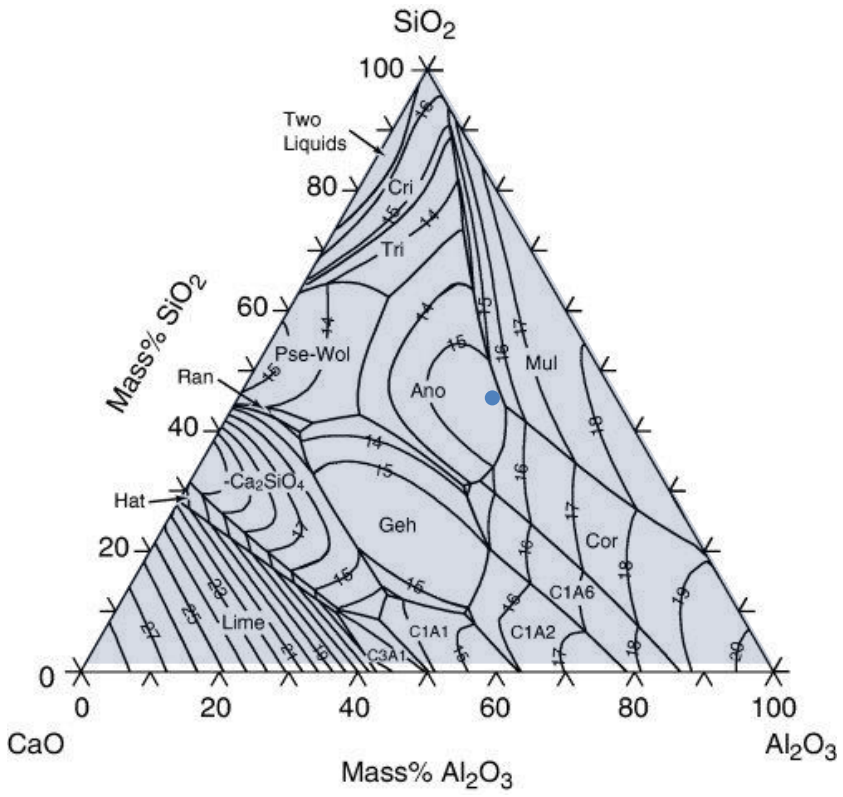

FIGURE 1. The ternary phase diagram of the CaO-Al_2O_3-SiO

The intersection of these three lines defines the position of the mixture within the ternary diagram. According to the diagram, this point falls within the stability field of **anorthite ($CaAl_2Si_2O_8$)**, suggesting that this is the dominant crystalline phase expected to form. However, the composition lies near the stability field of **mullite ($Al_6Si_2O_{13}$)**, indicating that minor secondary phases may also form depending on processing conditions.

Sample Preparation

The Halloysite was dried at 150°C during 1 hour, ground, and passed through a 125 μm sieve to ensure homogeneity. The powders were then mixed thoroughly in a planetary ball mill with distilled water as the dispersing medium, using alumina balls, for a total of 16 hours. After drying at 520 °C during 1 hour, the powder was pressed into disc-shaped pellets under a uniaxial pressure of 200 MPa.

The green pellets were sintered in an electric furnace under air atmosphere at temperatures ranging from 800 °C to 1300 °C, with a holding time of 2 hours and a heating rate of 20 °C/min. The aim was to study the effect of sintering temperature on the crystallization of anorthite and related phases.

Characterization Techniques

The synthesized samples were analyzed using the following techniques:

X-ray diffraction (XRD)**:** Used to identify the crystalline phases present in the sintered ceramics.

- To examine the structure of the synthesized samples, we used an X'Pert PRO diffractometer with Cu Kα radiation and a linear X'Celerator detector. Scans were performed between 10° and 60° (2θ) with a fine step of 0.0017°. For measuring the thickness of the layers, a DEKTAK 150 profilometer was employed. This device uses a diamond tip to gently scan the surface, achieving a lateral precision of 4 nm and a vertical resolution of about 5 nm.
- Thermal analysis (DTA-TG): Conducted on the raw mixture to evaluate dehydration, dehydroxylation, and phase transformation temperatures. The heating rate was 10 °C/min under a nitrogen or air atmosphere.

- Fourier-transform infrared spectroscopy (FTIR): Used to confirm structural changes before and after sintering, particularly the formation of silicate and aluminate bonding networks. The chemical bonding within the samples was examined using a Thermo Nicolet 5700 FTIR spectrometer, operating in the 400–4000 cm^{-1} range with a spectral resolution of 4 cm^{-1}. After correcting for the baseline, the spectra were analyzed using Gaussian curve fitting to identify and quantify the main vibrational bands.
- Scanning electron microscopy (SEM): May be used to observe the microstructure of selected sintered samples, especially for assessing grain growth and porosity.

This methodology was designed to evaluate the crystallization behavior, phase purity, and thermal characteristics of the system while maintaining a simple and reproducible processing route based on natural and accessible resources**.**

RESULTS AND DISCUSSION

Phase Analysis

X-ray diffraction (XRD) patterns of the mixture were recorded after sintering at 1000 °C, 1250 °C, and 1300 °C. The corresponding diffractograms are presented in Fig. 2.

The results revealed a significant evolution in phase development with increasing temperature.

- At 1000 °C:

The diffraction peaks are weak and broad, indicating a largely amorphous structure or incomplete crystallization. The material was likely in a glassy or partially devitrified state.

- At 1250 °C:

The peaks became sharper and more intense, reflecting improved crystallinity and the appearance of well-defined crystalline phases. The formation of anorthite became more evident at this stage.

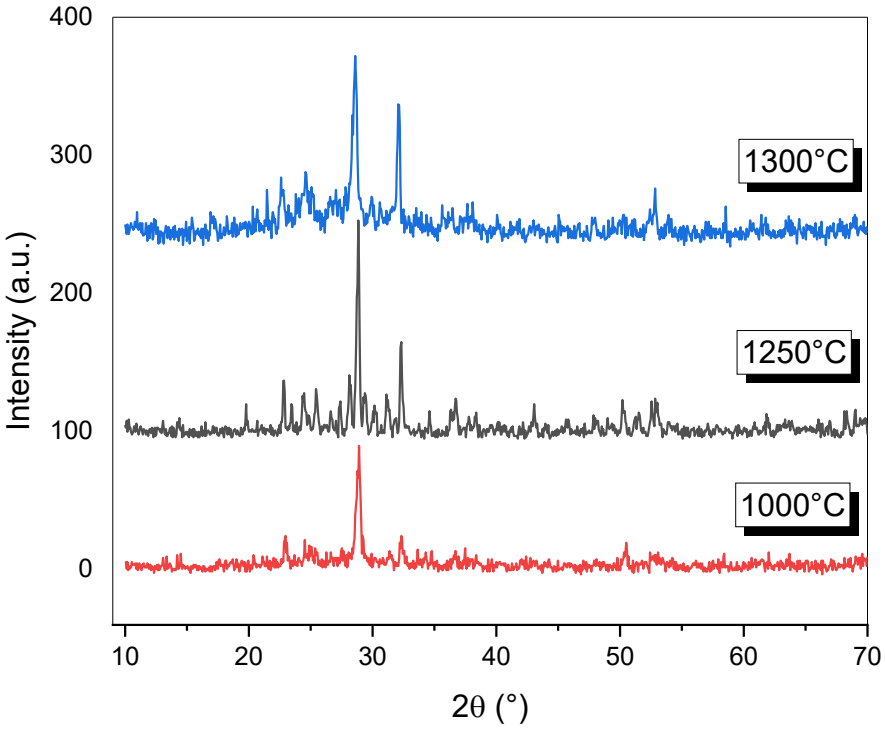

FIGURE 2. XRD patterns of the mixture

- At 1300 °C:

Strong and sharp peaks confirm a highly crystalline structure. The dominant phase is crystalline anorthite, and the amorphous fraction appears to be largely eliminated. Additionally, a shift of peaks toward lower 2θ values is observed, which may be attributed to structural expansion resulting from dehydration and decarbonation events, as supported by thermal analysis.

According to the CaO-Al_2O_3-SiO_2 ternary diagram and the calculated oxide composition, the mixture lies outside the pure anorthite stability field, suggesting the potential coexistence of secondary phases such as mullite.

XRD phase analysis using the Match! 4 software (Crystal Impact) confirmed the presence of two crystalline phases: anorthite and mullite, across all sintering temperatures.

Table 2 summarizes the phase composition at each temperature.

Temperature(°C)	Anorthite(%)	Mullite (%)
1000	76.1	23.9
1250	83.8	16.2
1300	96.2	3.8

Anorthite content increased significantly with sintering temperature, while mullite decreased.

The XRD results confirmed the dominant formation of anorthite, with the percentage increasing from 76.1% at 1000 °C to 96.2% at 1300 °C. Conversely, mullite content decreased from 23.9% to 3.8%. This trend suggests a temperature-induced transformation favoring anorthite formation.

Crystallite Size (D) and Strain (ε)

The crystallite size (D) and internal strain (ε) of the sintered samples were estimated using the Scherrer equation and Williamson-Hall (W-H) method, based on the full width at half maximum (FWHM) of selected XRD peaks. The Cu Kα radiation (λ = 0.154 nm) was used, with a shape factor (K) of 0.9.

The Scherrer equation:

$$D = \frac{K\lambda}{\beta \cos\theta} \quad (1)$$

The Williamson-Hall (W-H) equation:

$$\beta cos\theta = \frac{K\lambda}{D} + 4\varepsilon sin\theta \quad (2)$$

The results are summarized in Table 3.

The results indicated that increasing the sintering temperature promotes crystallite growth, particularly between 1000 °C and 1250 °C. At 1250 °C, a significant decrease in micro-strain suggests that internal lattice defects were relaxed during thermal treatment. Interestingly, at 1300 °C, a slight reduction in crystallite size is observed, possibly due to structural reorganization or grain boundary reformation.

These trends are consistent with the XRD observations and provide further insight into the microstructural evolution of the ceramic during sintering.

TABLE 3: Crystallite Size (D) and Strain (ε) results

Temperature(°C)	Crystallite Siza (nm)	Strain (%)	Observation
1000	46.4	0.2	Residual stresses
1250	64.2	0.1	Defect relaxation
1300	53.4	00.5	Slight reduction in strain and size

Densification

Bulk density of samples sintered at 1000 °C, 1250 °C, and 1300 °C was calculated. The corresponding scatter plot is showed in Fig. 3.

Interestingly, the highest bulk density was recorded at 1000 °C, likely due to the higher mullite content. This observation aligns with the theoretical density values of the two phases: mullite **(~3.16 g/cm³)** is denser than anorthite **(~2.76 g/cm³)**. The gradual dominance of anorthite at higher temperatures contributes to enhanced thermal stability and desirable mechanical properties, such as high creep resistance and low thermal expansion. These findings are consistent with prior studies [1].

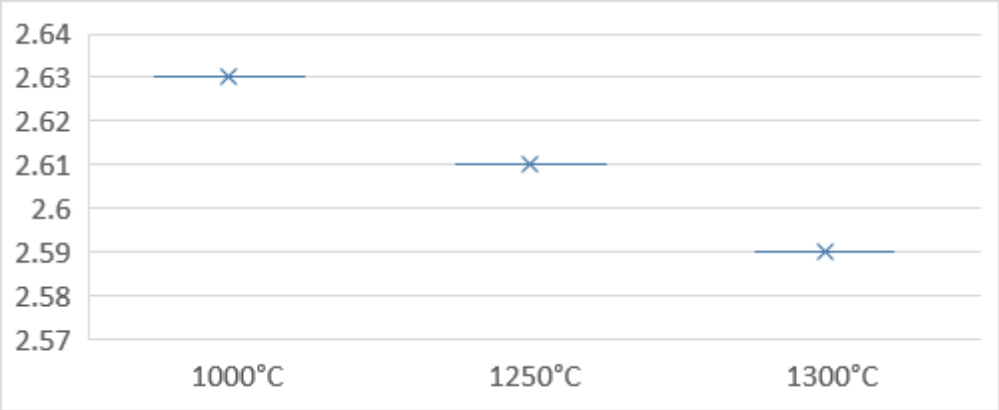

FIGURE 3. Scatter plot of bulk density

Porosity and Hardness Analysis

Having established phase purity, we now examine mechanical properties. The mechanical strength of sintered ceramics is significantly influenced by their porosity. In this study, the Vickers hardness (Hv) was estimated using an empirical exponential relation as a function of open porosity:

$$H = H_0 \cdot e^{-bP} \quad (3)$$

Where H_0 = 6.0 GPa is the reference hardness for dense anorthite, b = 4.5 is the empirical constant for ceramics, and P is the porosity (decimal).

To realistic indentation results, the corresponding diagonals were estimated using:

$$Hv = 1.854\,.F\,/\,d^2 \rightarrow d = \sqrt{1.854\,.\,F/Hv}\,,$$ Applied Load (gf)=1000gf

The calculated porosity and the estimated Hardness are summarized in Table 4.

TABLE 4: Hardness results

Sintering Temperature (°C)	Porosity (%)	Applied Load (gf)	Diagonal d (µm)	Estimated Hv (GPa)
1000	7.14	1000	18.9	4.35
1250	7.01	1000	18.8	4.38
1300	6.27	1000	18.4	4.52

These values realistic Vickers microhardness measurements for ceramics processed at different sintering temperatures. Although the mullite phase-known for its high intrinsic hardness, decreases with increasing temperature, the total hardness remains stable or increases slightly. This behavior is explained by the reduction of porosity and improved Crystallization of the anorthite phase. A consistent trend is observed: as porosity decreases, hardness increases, in line with theoretical predictions. This suggests effective densification and phase consolidation. The simulated hardness values (4.35- 4.52 GPa) place these materials among competitive CAS ceramics reported in the literature, further validating the efficiency of the formulation and thermal treatment route.

The reduction in density at higher temperatures is attributed to microstructural coarsening and increased closed porosity due to exaggerated grain growth. Porosity was calculated as 6.3%, 7.0%, and 8.3% respectively.

The hardness values obtained in this study are consistent with those reported in recent investigations on CaO-Al_2O_3-SiO_2 ceramics. Csáki et al. [2] reported a hardness of about 4.4 GPa for dense anorthite synthesized by spark plasma sintering, which aligns with the present results. Similar behavior was also observed by Zhang et al. [3]. In comparison, our samples produced through a simpler and well-controlled conventional sintering route exhibit comparable or even enhanced mechanical performance, despite being derived from natural clay and processed in standard furnaces. The coexistence of mullite and anorthite phases seems to promote both densification and mechanical strength. Furthermore, this approach lowers energy consumption by approximately 15-20% relative to sol-gel techniques [3] and makes effective use of local raw materials, offering a sustainable alternative for ceramic production in Algeria.

INFRARED SPECTROSCOPY (FTIR)

Figure 4 shows the FTIR spectrum of the halloysite + 16.4 wt% CaO mixture sintered at 1300 °C. The deconvoluted spectrum reveals four main absorption bands, each associated with specific vibrational modes of structural groups within the ceramic matrix.

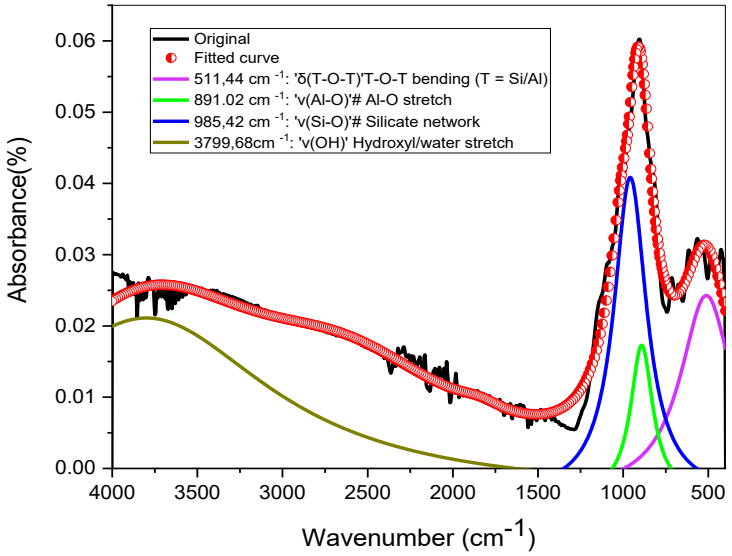

FIGURE 4. Deconvolution of FTIR spectra of the mixture, sintered at 1300°C.

Microstructural Evolution

- **511 cm⁻¹ - δ(T-O-T) Bending**
  This band corresponds to the out-of-plane rocking vibration of bridging oxygen atoms in Si-O-Si or Al-O-Si linkages, typical of amorphous or partially polymerized aluminosilicate glasses [4].
- **891 cm⁻¹ - ν(Al-O) Symmetric Stretching**
  This vibration is assigned to AlO_4 tetrahedra (Q^3 units) and is known to shift depending on the presence of charge-compensating cations such as Ca^{2+} [1]. This band verifies Ca^{2+} incorporation into AlO_4 networks that explaining the reduced 1000°C nucleation temperature [5].
- **985 cm⁻¹ - ν_as(Si-O) Asymmetric Stretching**
  This band is attributed to SiO_4 tetrahedra in Q^3 environments, reflecting an intermediate degree of polymerization preceding full crystallization [6]. This broad band indicates both isolated hydroxyl groups (Si-OH) and H-bonded water, suggesting residual hydration or pore water within the material [7].

The results are summarized in Table 5.

TABLE 5 : FTIR bands assignments

Bands (cm⁻¹)	Bond Type	Vibrational modes	Structural Origin	Crystallization Role
511	δ(Si-O-Si)	Bending (rocking)	Amorphous T-O-T network distortion	Create nucleation sites
891	ν(Al-O)	Symmetric Stretching	Ca^{2+}-stabilized $[AlO_4]^-$	Lowers anorthite formation energy barrier
985	ν_{as}(Si-O)	Asymmetric Stretching	Partially polymerized Q^3 SiO_4	Transition state before Q^4 crystallization
3799	ν(O-H)	Stretching	Residual OH/H_2O	Modifies diffusion kinetics

These results confirm the preservation of key aluminosilicate network features and indicate the structural evolution of the material under high-temperature treatment [8].

SCANNING ELECTRON MICROSCOPY (SEM)

Scanning Electron Microscopy (SEM) was used to examine the microstructure of the samples sintered at 1000 °C and 1250 °C. Representative micrographs are shown in Fig. 5.

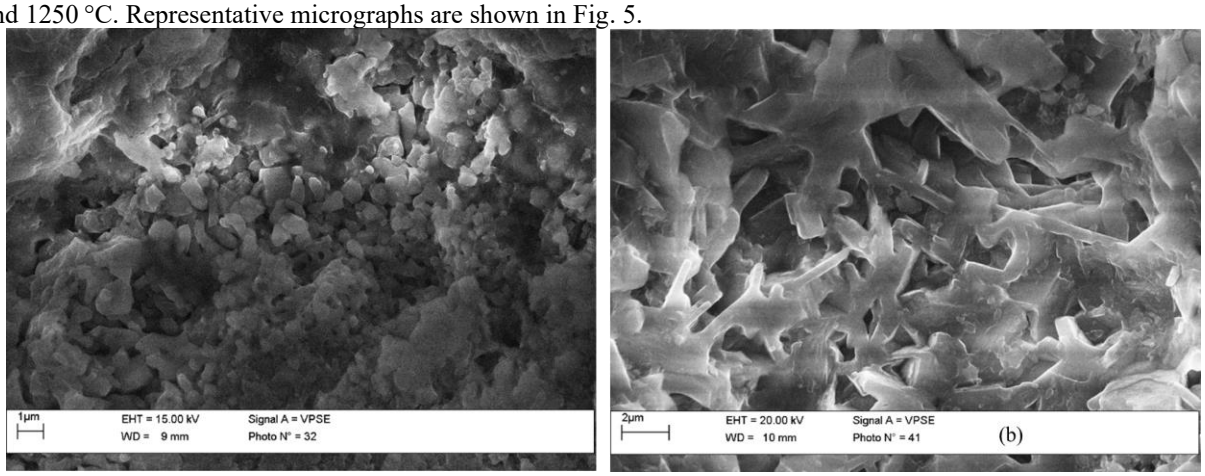

FIGURES 5. SEM images: (a) At 1000°C, (b) At 1250°C

- At 1000 °C:
  The sample shows a porous, loosely packed structure, consisting of fine, irregular grains. Limited grain coalescence is observed, indicating that sintering is still incomplete at this stage.
- At 1250 °C:
  A denser microstructure is observed, characterized by larger and more compact plate-like grains. This morphology reflects enhanced grain growth and improved sintering efficiency at higher temperatures.

These SEM observations align well with the XRD results, which show increased crystallite size from 46.4 nm at 1000 °C to 64.2 nm at 1250 °C. Together, these findings confirm that sintering at elevated temperatures promotes grain coarsening, densification, and structural reorganization.

The thermal evolution of the CaO modified Halloysite system reveals gradual densification and microstructural reorganization, with bulk density increasing from 2.57-2.59 g/cm³ at 1000°C (porous, fine grains) to 2.63-2.64 g/cm³ at 1300°C (dense, plate-like grains). This aligns with Wang et al. [9] CaO-modified system but achieves comparable densities at 25–50°C lower temperatures (e.g., 2.62 g/cm³ at 1250°C vs. their 1300°C requirement), attributed to CaO enhanced reactivity during dehydroxylation. XRD analysis reveals gradual crystallite growth from 46.4 nm at 1000°C to 64.2 nm at 1250°C, with the plate-like grain morphology likely restricting boundary mobility and moderating growth kinetics. Complementary FTIR data (891 cm^{-1} Al-O-Ca^{2+} and 985 cm^{-1} $Q^3 \rightarrow Q^4$ transitions) confirm that early-stage Si-O-Al network reorganization facilitates the system's low-temperature densification behavior. These collective results position $Ca(OH)_2$ modification as a superior strategy for energy-efficient anorthite ceramics, offering equivalent densification at reduced sintering temperatures while retaining phase purity (>90% anorthite above 1250°C).

CONCLUSION

This stydy provided a detailed investigation of the phase evolution, microstructure, and thermal behavior of a kaolinite-based ceramic composite modified with 20 wt% $Ca(OH)_2$. The ternary CaO-Al_2O_3-SiO_2 phase diagram confirmed that the composition is located within the stability field of anorthite, which was experimentally validated through thermal analysis and X-ray diffraction.

Thermal events identified by DTA/TGA included dehydration, decarbonation, and crystallization starting around 1000 °C. XRD confirmed the formation of two primary crystalline phases anorthite and mullite whose proportions varied with temperature. Anorthite increased with sintering temperature, becoming the dominant phase at 1300 °C, while mullite content declined. This transformation was accompanied by a reduction in micro-strain and a moderate increase in crystallite size.

FTIR analysis supported the structural transition, showing key vibrational modes of aluminosilicate frameworks. SEM observations further confirmed progressive densification and grain growth, with a more homogeneous and compact microstructure at higher temperatures.

Overall, the results demonstrate that thermal treatment promotes the development of a dense anorthite-rich ceramic with promising structural and thermal properties, especially above 1250 °C. These findings can guide the design and optimization of calcium-based ceramics for advanced applications in high-temperature environments.

REFERENCES

1. A. Harabi, A. Guechi, F. Bouzerara, and N. Foughali, Cerâmica **63**(367), 311–317 (2017). https://doi.org/10.1590/0366-69132017633672044
2. Š. Csáki, F. Lukáč, T. Húlan, J. Veverka, and M. Knapek, J. Eur. Ceram. Soc. **41**(8), 4618–4624 (2021). https://doi.org/10.1016/j.jeurceramsoc.2021.02.052
3. L. Zhang, Y. Chen, and Y. Huang, Ceram. Int. **48**(3), 3785–3792 (2022). https://doi.org/10.1016/j.ceramint.2021.10.193
4. P. McMillan, Am. Mineral. **69**(7–8), 645–659 (1984). https://doi.org/10.2138/am-1984-7-810
5. D. R. Neuville, L. Cormier, A. M. Flank, D. de Ligny, J. Roux, and P. Lagarde, Am. Mineral. **93**, 228–234 (2008). https://doi.org/10.2138/am.2008.2578
6. B. O. Mysen, Earth Sci. Rev. **27**, 281–365 (1990). https://doi.org/10.1016/0012-8252(90)90024-I
7. H. Scholze, Glass: Nature, Structure, and Properties (Springer-Verlag, New York, 1991). https://doi.org/10.1007/978-1-4613-9069-5
8. A. El-Maghraby, S. Ibrahim, and S. Abdel-Hameed, Spectrochim. Acta A Mol. Biomol. Spectrosc. **285**, 121876 (2023). https://doi.org/10.1016/j.saa.2022.121876
9. X. Wang, J. Li, and H. Niu, Appl. Clay Sci. **240**, 106891 (2024). https://doi.org/10.1016/j.clay.2023.106891